Proceedings of the ASME 2015 Dynamic Systems and Control Conference
DSCC2015
October 28-30, 2015 Columbus, Ohio, USA

STABLE ROBUST ADAPTIVE IMPEDANCE CONTROL OF A PROSTHETIC LEG

Vahid Azimi
Department of Electrical Engineering and Computer Science, Cleveland State University, Cleveland, OH, USA
Email: v.azimi@csuohio.edu

Dan Simon
Department of Electrical Engineering and Computer Science, Cleveland State University, Cleveland, OH, USA
Email: d.j.simon@csuohio.edu

Hanz Richter
Department of Mechanical Engineering, Cleveland State University, Cleveland, OH, USA
Email: h.richter@csuohio.edu

ABSTRACT

We propose a nonlinear robust model reference adaptive impedance controller for an active prosthetic leg for transfemoral amputees. We use an adaptive control term to consider the uncertain parameters of the system, and a robust control term so the system trajectories converge to a sliding mode boundary layer and exhibit robustness to variations of ground reaction force (GRF). The boundary layer not only compromises between control chattering and tracking performance, but also bounds the parameter adaptation to prevent unfavorable parameter drift. We also prove the stability of the controller for the robotic system in the case of non-scalar boundary layer trajectories using Lyapunov stability theory and Barbalat's lemma. The acceleration-free regressor form of the system removes the need to measure the joint accelerations, which would otherwise introduce noise in the system. We use particle swarm optimization (PSO) to optimize the design parameters of the controller and the adaptation law. The PSO cost function is comprised of control signal magnitudes and tracking errors. PSO achieves a 8% improvement in the objective function. Finally, we present simulation results to validate the effectiveness of the controller. We achieve good tracking of joint displacements and velocities for both nominal and perturbed values of the system parameters. Variations of ±30% on the system parameters result in an increase of the cost function by only 3%, which confirms the robustness of the controller.

INTRODUCTION

The number of people with limb loss in the United States is estimated at about two million [1]. Amputation has several causes, including accidents, cancer, diabetes, vascular disease, birth defects, and paralysis [1, 2]. Amputation includes transtibial (below the knee), transfemoral (above the knee), foot amputations, and hip and knee disarticulations (amputation through the joint). Amputees can use prosthetic legs in an attempt to restore normal walking gait.

There are three general types of prosthetic legs: passive (no electronic control), active (motor control), and semi-active (control without motors) [3]. Technology has provided advanced prosthetic legs to restore able-bodied gait and to enable increased activity levels for amputees. Compared to passive and semi-active prostheses, active prostheses enable more natural walking.

The Power Knee was the first commercially available active transfemoral prosthesis [3-5]. A combination knee / ankle prosthesis, in which both joints are active, was recently developed at Vanderbilt University and is in the process of commercialization [6]. Researchers have recently concentrated on the design and control of these and other active prostheses [7-11]. Recent years have witnessed numerous advancements in control and modeling for prosthetic legs [12-14].

A prosthesis can be viewed as a robotic system. A robot's environment and the robot itself can be viewed as a mechanical admittance and impedance. Choosing the controller to be an impedance or admittance controller depends on the robot interface. Based on its design, the robot may have admittance or impedance type interfaces [15-16]. These factors motivate the development of impedance control [17].

Since modeling inaccuracies are unavoidable, robust controllers can reduce these effects on performance and stability [18, 19]. Robust controllers try to achieve a certain level of performance in the presence of modeling uncertainties, whereas adaptive controllers try to achieve performance with learning and adaptation. Adaptive controllers may be preferable to non-adaptive robust controllers because adaptive controllers can handle system uncertainties that change with time. Non-adaptive robust controllers require a priori knowledge of the bounds of the parameter perturbations, whereas adaptive approaches do not. In a robust controller, good a priori estimates of the system parameters are required, while in an adaptive controller these parameters are estimated online.

The aforementioned advantages of adaptive control, along with the availability of able-bodied human impedance properties and uncertain robot model parameters, has given rise to impedance model reference adaptive control for robotics [20-22]. Pure adaptive control approaches may become unstable when disturbances, unmodeled dynamics, or external forces affect the system. Robust control can alleviate instabilities in these cases [23-30]. Several adaptive control schemes and

sliding surface theories have also been proposed for robotics [31-34].

The contribution of this research is the design and stability analysis of a nonlinear robust model reference adaptive impedance controller for a prosthetic leg for transfemoral amputees. We use robust adaptive control to deal with parameter uncertainties and GRF variations so that the closed-loop system converges to a target impedance model. Among related research [20-22], our work has the most similarity to the controllers in [21].

New contributions in this paper include blending adaptive and robust control to reduce the effects of unknown parameters on system performance, and to obtain good robustness against GRF variations (environment interaction), and proving the stability of the proposed method. We extend the work in [21] by defining a boundary layer trajectory s_Δ to trade off control chattering and tracking accuracy, and to create an adaptation dead zone to prevent unfavorable parameter drift. We define a boundary layer to stop parameter adaptation when tracking errors reach a satisfactory level, so the system trajectories converge inside this layer. We prove the stability of the closed-loop robotic system which uses a non-scalar boundary layer trajectory via Barbalat's lemma and Lyapunov theory. (Note that the stability analysis of the robust adaptive controller for the scalar and non-robotic case was presented in [31].) Furthermore, we use PSO to optimize the control design parameters. The PSO cost function includes control signal magnitudes and tracking errors, and PSO reduces the cost function by 8%. Numerical results show that the proposed system has good robustness to system uncertainties. When we change the system parameters by −30% and +30%, the total cost increases by only 1.6% and 2.6% respectively, and the tracking performance component of the cost increases by 2.5% and 6.5% respectively.

The following section describes the dynamic model of the prosthetic leg. The next section presents the design of the controller and proves its stability. The next section presents simulation and robustness simulation results. The final section includes discussion, concluding remarks, and future work.

PROSTHETIC LEG MODEL

We present a model for the prosthetic leg with three rigid links and three degrees of freedom. The prosthetic component is modeled as an active transfemoral (above-knee) prosthesis. This proposed model has a prismatic-revolute-revolute (PRR) joint structure as illustrated in Fig. 1. Human hip and thigh motion are emulated by a prosthesis test robot [13, 14, 35]. The vertical degree of freedom represents human vertical hip motion, the first rotational axis represents human angular thigh motion, and the second rotational axis represents prosthetic angular knee motion.

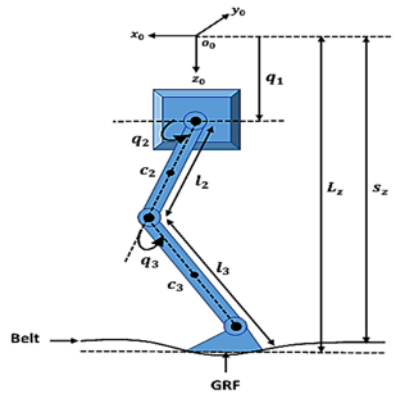

Fig. 1: Prosthetic leg model with rigid ankle

The three degree-of-freedom model can be written as follows [13]:

$$M\ddot{q} + C\dot{q} + g + R = u - T_e \tag{1}$$

where $q^T = [q_1 \quad q_2 \quad q_3]$ is the vector of generalized joint displacements (q_1 is the vertical displacement, q_2 is the thigh angle, and q_3 is the knee angle); $M(q)$, $C(q,\dot{q})$, $g(q)$, and $R(q,\dot{q})$ are the inertia matrix, Coriolis and Centripetal matrix, gravity vector, and nonlinear damping vector, respectively; T_e is the effect of the combined horizontal (F_x) and vertical (F_z) components of the GRF on each joint; u is the control signal that comprises the active control force at the hip and the active control torques at the thigh and knee.

We use a treadmill as the walking surface of the prosthesis test robot. We model the treadmill belt as a mechanical stiffness so the reaction forces from the treadmill are functions of the belt deflection [14]. T_e is the effect of the GRF on the three joints and is given as follows [35]:

$$L_z = q_1 + l_2\sin(q_2) + l_3\sin(q_2 + q_3) \tag{2}$$

$$F_z = \begin{cases} 0 & , \quad L_z < s_z \\ k_b(s_z - L_z) & , \quad L_z > s_z \end{cases} \tag{3}$$

$$F_x = \beta F_z \tag{4}$$

$$T_e = \begin{bmatrix} F_z \\ F_z(l_2\cos(q_2) + l_3\cos(q_2+q_3)) - F_x(l_2\sin(q_2) + l_3\sin(q_2+q_3)) \\ F_z(l_3\cos(q_2+q_3)) - F_x(l_3\sin(q_2+q_3)) \end{bmatrix} \tag{5}$$

where l_2 and l_3 are the length of the thigh and shank respectively; L_z is the vertical position of bottom of the foot in the world frame (x_0, y_0, z_0); s_z is the treadmill standoff (vertical distance between the origin of the world frame and the belt); k_b is the belt stiffness; and β is the belt friction coefficient (see Fig. 1). The states and control inputs are defined as

$$\begin{aligned} x^T &= [q_1 \quad q_2 \quad q_3 \quad \dot{q}_1 \quad \dot{q}_2 \quad \dot{q}_3] \\ u^T &= [f_{hip} \quad \tau_{thigh} \quad \tau_{knee}] \end{aligned} \tag{6}$$

We convert the left hand side of Eq. (1) into the following parameterized form [36, 37]:

$$M\ddot{q} + C\dot{q} + g + R = Y'(q, \dot{q}, \ddot{q})p' \tag{7}$$

where $Y'(q, \dot{q}, \ddot{q}) \in R^{n\times r}$ is a regressor matrix that is a function of the joint displacements, velocities, and accelerations; n is the number of rigid links (n is equal to 3 in our case; see Eq. (6)); and $p' \in R^r$ is a parameter vector.

ROBUST ADAPTIVE IMPEDANCE CONTROL

The main contribution of this research is the design of a nonlinear robust adaptive impedance controller using a boundary layer and a sliding surface to track hip displacement, knee and thigh angles, and their velocities, in the presence of parameter uncertainties. We desire the closed-loop system to imitate the biomechanical properties of able-bodied walking and to provide near-normal gait for amputees. Therefore, we define a target impedance model with characteristics that are similar to those of able-bodied walking [37]:

$$M_r(\ddot{q}_r - \ddot{q}_d) + B_r(\dot{q}_r - \dot{q}_d) + K_r(q_r - q_d) = -T_e \tag{8}$$

where the desired mass M_r, the damping coefficient B_r, and the spring stiffness K_r are the positive definite matrices of the target model; and $q_r \in R^n$ and $q_d \in R^n$ are the state vectors of the reference model and the desired trajectory respectively. For the sake of simplicity, we suppose these matrices are diagonal:

$$\begin{aligned} M_r &\in R^{n\times n} = \text{diag}\,(M_{11} \quad M_{22} \quad \dots \quad M_{nn}) \\ B_r &\in R^{n\times n} = \text{diag}\,(B_{11} \quad B_{22} \quad \dots \quad B_{nn}) \\ K_r &\in R^{n\times n} = \text{diag}(K_{11} \quad K_{22} \quad \dots \quad K_{nn}) \end{aligned}$$

In the model in Eq. (7), the regressor matrix depends on the joint acceleration. In practice the joint acceleration measurements can be very noisy, so $Y'(q, \dot{q}, \ddot{q})$ might not be convenient for real-time implementation. Consequently, to avoid the need to measure the joint accelerations, we define error and signal vectors s and v respectively, based on Slotine and Li's approach [33, 34, 36, 37]:

$$s = \dot{e} + \lambda e \tag{9}$$
$$v = \dot{q}_r - \lambda e \tag{10}$$
$$e = q - q_r \tag{11}$$
$$\lambda = \text{diag}(\lambda_1, \lambda_2, \dots, \lambda_n)\,, \lambda_i > 0 \tag{12}$$

In place of the regressor model of Eq. (7), we define an acceleration-free regressor model as follows:

$$M\ddot{q} + C\dot{q} + g + R = Y(q, \dot{q}, v, \dot{v})p \tag{13}$$

where $Y(q, \dot{q}, v, \dot{v})$ is a linear combination of $q, \dot{q}, v$, and $\dot{v}$. The regressor matrix $Y(q, \dot{q}, v, \dot{v})$ and the associated parameter vector p have many realizations; one such realization is given as follows:

$$p = \begin{bmatrix} m_1 + m_2 + m_3 \\ m_3 l_2 + m_2 l_2 + m_2 c_2 \\ m_3 c_3 \\ I_{2z} + I_{3z} + m_2 {c_2}^2 + m_3 {c_3}^2 + m_2 {l_2}^2 + m_3 {l_2}^2 + 2m_2 c_2 l_2 \\ m_3 c_3 l_2 \\ m_3 {c_3}^2 + I_{3z} \\ b \\ f \end{bmatrix} \tag{14}$$

$$Y(q, \dot{q}, v, \dot{v}) = \begin{bmatrix} \dot{v}_1 - g & Y_{12} & Y_{13} & 0 & 0 & 0 & 0 & \text{sgn}(\dot{q}_1) \\ 0 & Y_{22} & Y_{23} & \dot{v}_2 & Y_{25} & \dot{v}_3 & \dot{q}_2 & 0 \\ 0 & 0 & Y_{33} & 0 & Y_{35} & \dot{v}_{2+}\dot{v}_3 & 0 & 0 \end{bmatrix}$$

$$\begin{aligned} Y_{12} &= \dot{v}_2 \cos(q_2) - v_2 \dot{q}_2 \sin(q_2) \\ Y_{13} &= (\dot{v}_2 + \dot{v}_3)\cos(q_3 + q_2) \\ &\quad -(v_2\dot{q}_3 + v_2\dot{q}_2 + v_3\dot{q}_2 + v_3\dot{q}_3)\sin(q_3 + q_2) \\ Y_{22} &= (\dot{v}_1 - \text{g})\cos(q_2) \\ Y_{23} &= Y_{33} = (\dot{v}_1 - g)\cos(q_3 + q_2) \\ Y_{25} &= (2\dot{v}_2 + \dot{v}_3)\cos(q_3) - (v_2\dot{q}_3 + v_3\dot{q}_3 + v_3\dot{q}_2)\sin(q_3) \\ Y_{35} &= \dot{v}_2 \cos(q_3) + \sin(q_3)\, v_2 \dot{q}_2 \end{aligned} \tag{15}$$

By substituting Eqs. (9), (10), (11), and (12) in Eq. (1), we rewrite the model in the following form:

$$M\dot{s} + Cs + g + R + M\dot{v} + Cv = u - T_e \tag{16}$$

Since the system of Eq. (1) is a second-order dynamic system, the error vector of Eq. (9) is derived from the following first-order sliding surface:

$$s = \left(\frac{d}{dt} + \lambda\right) e \tag{17}$$

where s is as n-element vector. Perfect tracking $q = q_r$ ($e = 0$) is equivalent to $s = 0$. In order to reach the sliding manifold $s = 0$ in finite time, the following reaching condition must be attained [31]:

$$\text{sgn}(s)\dot{s} \le -\gamma \tag{18}$$

where the inequality is interpreted element-wise, and γ is an n-element vector such that $\gamma = [\gamma_1 \quad \gamma_2 \quad \cdots \quad \gamma_n]^T$ and $\gamma_i > 0$. From Eq. (18) we see that in the worst case, $\text{sgn}(s)\dot{s} = -\gamma$, so we can calculate the worst-case reaching time to $s = 0$ of the tracking error trajectories as follows:

$$\begin{aligned} \int_{s(0)}^{0} \text{sgn}(s)ds = -\gamma \int_0^T dt \rightarrow |s(0)|\text{sgn}(s) = \gamma\, T \\ T = \frac{s(0)}{\gamma} \end{aligned} \tag{19}$$

which represents n different reaching times, where $s(0)$ is the initial error, and the division $s(0)/\gamma$ is interpreted element-wise. It is seen from Eq. (19) that increasing γ results in a smaller reaching time T.

Since the parameters of the system are unknown, we use a control law [31] to not only consider parameter uncertainties but also to satisfy the reaching condition of Eq. (18):

$$u = \hat{M}\dot{v} + \hat{C}v + \hat{g} + \hat{R} + \hat{T}_e - K_d \text{sgn}(s) \tag{20}$$

where $\hat{M}$, $\hat{C}$, $\hat{g}$, $\hat{R}$, and $\hat{T}_e$ are estimates of M, C, g, R, and T_e respectively; K_d is a robust control design matrix with $K_d = \text{diag}(K_{d_1}, K_{d_2}, \dots, K_{d_n})$, and $K_{d_i} > 0$. Since the function $\text{sgn}(s)$ is discontinuous and causes control chattering, the saturation function $\text{sat}(s/\text{diag}(\varphi))$ (see Fig. 2) promises to provide better performance than the sign function. (Note that the division and saturation operations for s and $\text{diag}(\varphi)$ in the term $\text{sat}(s/\text{diag}(\varphi))$ are interpreted element-wise and $\text{diag}(\varphi)$ is an n-element vector.) So we modify the control law of Eq. (20) as follows:

$$u = \hat{M}\dot{v} + \hat{C}v + \hat{g} + \hat{R} + \hat{T}_e - K_d \,\text{sat}(s/\text{diag}(\varphi)) \tag{21}$$

where the diagonal elements of φ are the widths of the saturation function.

The control law of Eq. (21) comprises two different parts. The first part, $\hat{M}\dot{v} + \hat{C}v + \hat{g} + \hat{R}$, is an adaptive control term that is responsible for handling the uncertain parameters. The second part, $\hat{T}_e - K_d \,\text{sat}(s/\text{diag}(\varphi))$, is a robust control term that is responsible for satisfying the condition of Eq. (18) and the variations of the external inputs T_e. Substituting Eq. (21) into Eq. (16) and defining $\tilde{M} = M - \hat{M}$, $\tilde{C} = C - \hat{C}$, $\tilde{g} = g - \hat{g}$, $\tilde{R} = R - \hat{R}$, and $\tilde{p} = p - \hat{p}$, we derive the closed-loop system as follows:

$$M\dot{s} + Cs + K_d \text{sat}(s/\text{diag}(\varphi)) + \left(T_e - \hat{T}_e\right) = -(\tilde{M}\dot{v} + \tilde{C}v + \tilde{g} + \tilde{R}) \tag{22}$$

We can separate the right hand side of Eq. (22) into two different parts: the regressor matrix $Y(q, \dot{q}, v, \dot{v})$ and the parameter estimation error vector $\tilde{p}$. Therefore, we can present Eq. (22) in the following regressor (linear parametric) form:

$$M\dot{s} + Cs + K_d \text{sat}(s/\text{diag}(\varphi)) + \left(T_e - \hat{T}_e\right) = -Y(q, \dot{q}, v, \dot{v})\tilde{p} \tag{23}$$

Next, to trade off control chattering and tracking accuracy, and to create an adaptation dead zone to prevent unfavorable parameter drift, we define a trajectory s_Δ as follows [31, 36]:

$$s_\Delta = \begin{cases} 0 & , \quad |s| \le \text{diag}(\varphi) \\ s - \varphi \,\text{sat}(s/\text{diag}(\varphi)) & , \quad |s| > \text{diag}(\varphi) \end{cases} \tag{24}$$

where s_Δ is as n-element vector; the region $|s| \le \text{diag}(\varphi)$ is the boundary layer and the inequality is interpreted element-wise; and the diagonal elements of φ are the boundary layer thicknesses and the widths of the saturation function so that $\varphi = \text{diag}(\varphi_1, \varphi_2, \dots, \varphi_n)$ and $\varphi_i > 0$. We depict s_Δ and the function $\text{sat}(s/\text{diag}(\varphi))$ for a single link in Fig. 2.

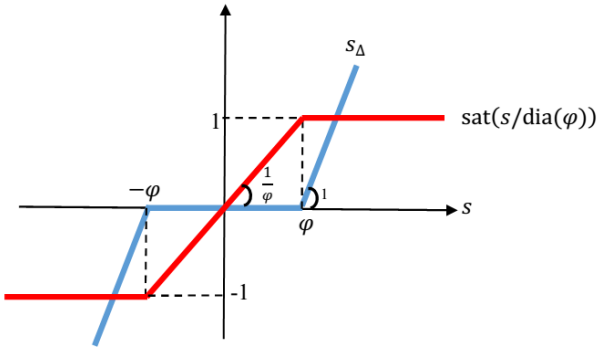

Fig. 2: Saturation function and trajectory s_Δ for a single link

To drive a stable adaptation law, we present a scalar positive definite Lyapunov function as follows [36]:

$$V(s_\Delta, \tilde{p}) = \frac{1}{2}({s_\Delta}^T M\, s_\Delta) + \frac{1}{2}(\tilde{p}^T \mu\, \tilde{p}) \tag{25}$$

where μ is a design parameter such that $\mu = \text{diag}(\mu_1, \mu_2, \dots, \mu_r)$, with $\mu_i > 0$. Note that even though s_Δ is not continuously differentiable, V is continuously differentiable because it is a quadratic function of s_Δ. We find the derivative of the Lyapunov function as follows:

$$\begin{aligned} \dot{V}(s_\Delta, \tilde{p}) &= \frac{1}{2}\left({\dot{s}_\Delta}^T M\, s_\Delta + {s_\Delta}^T M\, \dot{s}_\Delta\right) + \frac{1}{2}\left({s_\Delta}^T \dot{M} s_\Delta\right) + \\ &\quad \frac{1}{2}\left(\dot{\tilde{p}}^T \mu\, \tilde{p} + \tilde{p}^T \mu\, \dot{\tilde{p}}\right) \\ &= {s_\Delta}^T M\, \dot{s}_\Delta + \frac{1}{2}\left({s_\Delta}^T \dot{M} s_\Delta\right) + \dot{\tilde{p}}^T \mu\, \tilde{p} \end{aligned}$$

Inside the boundary layer $\dot{s}_\Delta = 0$, and outside of it $\dot{s}_\Delta = \dot{s}$, so

$$\begin{aligned} \dot{V}(s_\Delta, \tilde{p}) &= {s_\Delta}^T\left(-Cs - K_d sat(s/\text{diag}(\varphi)) + \left(\hat{T}_e - T_e\right) - \right. \\ &\quad \left. Y(q, \dot{q}, v, \dot{v})\tilde{p}\right) + \tfrac{1}{2}\left({s_\Delta}^T \dot{M} s_\Delta\right) + \dot{\tilde{p}}^T \mu\, \tilde{p} \\ &= -{s_\Delta}^T Cs + \frac{1}{2}\left({s_\Delta}^T \dot{M} s_\Delta\right) - {s_\Delta}^T K_d sat(s/\text{diag}(\varphi)) \\ &\quad + {s_\Delta}^T\left(\hat{T}_e - T_e\right) - {s_\Delta}^T Y(q, \dot{q}, v, \dot{v})\tilde{p} + \dot{\tilde{p}}^T \mu\, \tilde{p} \end{aligned}$$

In order to have an adaptation mechanism, we will constrain the term $\dot{\tilde{p}}^T \mu\, \tilde{p} - {s_\Delta}^T Y(q, \dot{q}, v, \dot{v})\tilde{p}$ to be equal to zero and in turn we can derive the update law as

$$\dot{\tilde{p}} = -\mu^{-1} Y^T(q, \dot{q}, v, \dot{v}) s_\Delta \tag{26}$$

Therefore, $\dot{V}(s_\Delta, \tilde{p})$ can be rewritten as follows:

$$\dot{V}(s_\Delta, \tilde{p}) = -{s_\Delta}^T C s + \frac{1}{2}\left({s_\Delta}^T \dot{M} s_\Delta\right) - {s_\Delta}^T K_d \operatorname{sat}(s/\operatorname{diag}(\varphi)) + {s_\Delta}^T\left(\hat{T}_e - T_e\right) \tag{27}$$

We see from (24) that if $|s| \le \operatorname{diag}(\varphi)$, then $s_\Delta = 0$ and $\dot{V}(s_\Delta, \tilde{p})$ tends to zero (inside the boundary layer). On the other hand, if $|s| > \operatorname{diag}(\varphi)$, then s_Δ is determined by the second condition of Eq. (24), in which case we see that $s = s_\Delta + \varphi \operatorname{sat}(s/\operatorname{diag}(\varphi))$ (outside the boundary layer). Substituting $s = s_\Delta + \varphi \operatorname{sat}(s/\operatorname{diag}(\varphi))$ into Eq. (27), we can write $\dot{V}(s_\Delta, \tilde{p})$ outside the boundary layer as

$$\dot{V}(s_\Delta, \tilde{p}) = \frac{1}{2}{s_\Delta}^T\left(\dot{M} - 2C\right)s_\Delta - {s_\Delta}^T C\varphi \operatorname{sat}(s/\operatorname{diag}(\varphi)) - {s_\Delta}^T K_d \operatorname{sat}(s/\operatorname{diag}(\varphi)) + {s_\Delta}^T\left(\hat{T}_e - T_e\right) \tag{28}$$

Matrix $\dot{M} - 2C$ is skew-symmetric, so ${s_\Delta}^T\left(\dot{M} - 2C\right)s_\Delta = 0$ and we can simplify $\dot{V}(s_\Delta, \tilde{p})$ as

$$\dot{V}(s_\Delta, \tilde{p}) = -{s_\Delta}^T(C\varphi + K_d) \operatorname{sat}(s/\operatorname{diag}(\varphi)) + {s_\Delta}^T\left(\hat{T}_e - T_e\right) \tag{29}$$

We then choose K_d and φ as the design parameters so that the term $C\varphi + K_d$ is lower bounded by a positive definite matrix $K_m I$ where K_m is a positive number. Note that $C\varphi + K_d \ge K_m I$ guarantees the positive-definiteness of $C\varphi + K_d$. We can then use Eq. (29) to write

$$\dot{V}(s_\Delta, \tilde{p}) \le -K_m {s_\Delta}^T \operatorname{sat}(s/\operatorname{diag}(\varphi)) + {s_\Delta}^T\left(\hat{T}_e - T_e\right) \tag{30}$$

It can be seen that ${s_\Delta}^T \operatorname{sat}(s/\operatorname{diag}(\varphi))$ is equal to the 1-norm of s_Δ, so we can write Eq. (30) as

$$\dot{V}(s_\Delta, \tilde{p}) \le -K_m \|s_\Delta\|_1 + {s_\Delta}^T\left(\hat{T}_e - T_e\right) \tag{31}$$

We now define $K_m = F_m + \gamma_m$, where $\left|\hat{T}_{e_i} - T_{e_i}\right| \le F_i \le F_m$, $F_m = \max(F_i)$, and $\gamma_m = \max(\gamma_i)$. We can then write Eq. (31) as follows:

$$\dot{V}(s_\Delta, \tilde{p}) \le -\gamma_m \|s_\Delta\|_1 - F_m \|s_\Delta\|_1 + {s_\Delta}^T\left(\hat{T}_e - T_e\right) \tag{32}$$

Noting that $\left|\hat{T}_{e_i} - T_{e_i}\right| \le F_i \le F_m$ and $s_{\Delta_i} \le \left|s_{\Delta_i}\right|$, we see that ${s_\Delta}^T\left(\hat{T}_e - T_e\right)$ in Eq. (32) is upper bounded by $F_m\|s_\Delta\|_1$, so we can write

$$\dot{V}(s_\Delta, \tilde{p}) \le -\gamma_m \|s_\Delta\|_1 \tag{33}$$

We thus see that outside the boundary layer (the second condition of Eq. (24)), the derivative of the Lyapunov function is negative semi-definite, which means that we can utilize Barbalat's lemma [36] to prove the asymptotic stability of the closed-loop system as follows.

Barbalat's lemma: If a candidate Lyapunov function $V = V(t, x)$ satisfies the following conditions:

I. $V(t, x)$ is lower-bounded.
II. $\dot{V}(t, x)$ is negative semi-definite.
III. $\ddot{V}(t, x)$ is bounded.

then $\dot{V}(t, x) \to 0$ as $t \to \infty$, which implies the asymptotic stability of the closed-loop system.

Theorem 1: According to Barbalat's lemma, the derivative of the Lyapunov function presented in (33) asymptotically converges to zero, which means that convergence of the system to the boundary layer is guaranteed.

Proof: Items I and II can be easily found from Eqs. (25) and (33), and from these two items we can conclude that V is bounded; therefore, all terms in V in Eq. (25), namely, s_Δ and $\tilde{p}$, are bounded. Since p is constant, $\hat{p}$ is bounded. Since s_Δ is bounded, s is bounded. The second derivative of V is $\ddot{V}(s_\Delta, \tilde{p}) \le -\gamma_m \frac{d}{dt}\|s_\Delta\|_1$ and in the worst case we have

$$\ddot{V}(s_\Delta, \tilde{p}) = -\gamma_m \frac{d}{dt}\|s_\Delta\|_1 = -\gamma_m \sum \frac{s_\Delta \dot{s}_\Delta}{|s_\Delta|} = \pm \gamma_m \sum \dot{s}_\Delta = \pm \gamma_m \sum \dot{s} \tag{34}$$

where $s_\Delta \ne 0$ (outside the boundary layer). Substituting $\dot{s}$ from Eq. (23) into Eq. (34) gives

$$\ddot{V}(s_\Delta, \tilde{p}) = \pm \gamma_m \sum M^{-1}\left(-Cs - K_d \operatorname{sat}(s/\operatorname{diag}(\varphi)) + \left(\hat{T}_e - T_e\right) - Y(q, \dot{q}, v, \dot{v})\tilde{p}\right) \tag{35}$$

We showed above that $\tilde{p}$ and s are bounded. Since s is bounded, e and $\dot{e}$ are bounded (Eq. (9)), and the boundedness of q_r, $\dot{q}_r$, and $\ddot{q}_r$ implies that q, $\dot{q}$, v, and $\dot{v}$ are bounded. Therefore, in Eq. (35), $M, C, \varphi, \tilde{p}, Y, \gamma_m, s$, and K_d are bounded. $\left|\hat{T}_e - T_e\right|$ is upper bounded by F_m, so we can conclude that $\ddot{V}$ is bounded. Consequently, as premises, I, II, and III in Barbalat's lemma hold, we conclude that $\dot{V}(s_\Delta, \tilde{p}) \to 0$ as $t \to \infty$. This implies that $-\gamma_m\|s_\Delta\|_1$ in Eq. (33) is equal to zero, so we conclude that the inequality of Eq. (33) can be written as the equality $\dot{V}(s_\Delta, \tilde{p}) = -\gamma_m\|s_\Delta\|_1$. We therefore have $\dot{V}(s_\Delta, \tilde{p}) \to 0 \Longmapsto -\gamma_m\|s_\Delta\|_1 \to 0 \Longmapsto s_\Delta \to 0$, which means that outside the boundary layer, the proposed controller guarantees the convergence of the trajectories of s to inside the boundary layer after the adaptation period. ■

The proposed robust adaptive controller reduces the effects of the system uncertainties compared to a basic adaptive controller, but results in a corresponding increase in the tracking error. This controller drives the system into the boundary layer and provides robustness against variations of the external effects of GRFs. Inside the boundary layer, the adaptation stops and the

estimated system parameters are constant. It should be noted that based on the stability analysis to get the asymptotic stability of the closed-loop system, K_d must be lower bounded by $C\varphi + F_m$ ($K_d \geq C\varphi + F_m + \gamma_m$). The robust model reference adaptive impedance controller structure is summarized in Fig. 3.

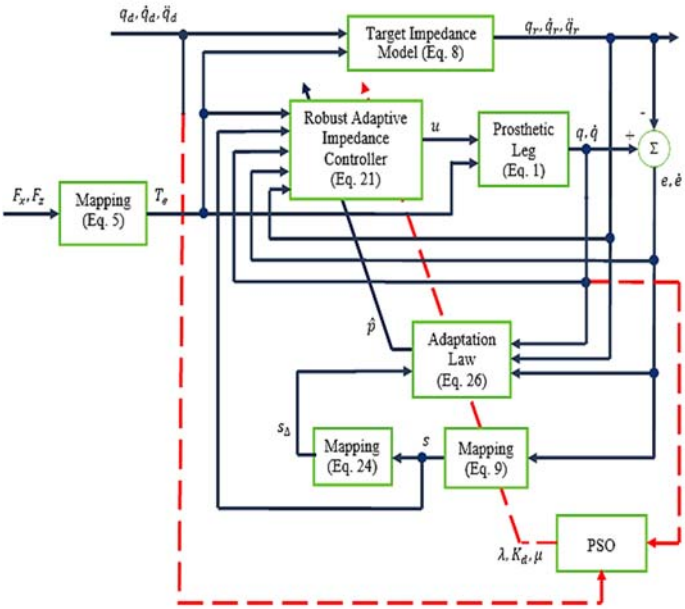

Fig. 3: Robust model reference adaptive impedance controller structure

Theorem 1 proves that trajectories of s are bounded inside the boundary layer. PSO optimizes the controller design parameters (λ, μ, and K_d) so that the errors between the states of the system and the desired trajectories ($\dot{q}_{di}$ and q_{di}) are minimized as quickly as possible, while preventing large magnitudes in the control signals. To achieve these goals, we define a PSO cost function. The tracking error portion of the cost, and the control portion of the cost, are defined as follows:

$$RMSE_i = \sqrt{\frac{1}{T}\int_0^T (x_i - r_{d_i})^2\, dt} \quad , \quad i = 1, \dots, 6 \tag{36}$$

$$RMSU_j = \sqrt{\frac{1}{T}\int_0^T u_j{}^2\, dt} \quad , \quad j = 1, \dots, 3 \tag{37}$$

where T is the time period (one stride), and x, r, and u are given as follows:

$$\begin{aligned} x^T &= [q_1 \quad q_2 \quad q_3 \quad \dot{q}_1 \quad \dot{q}_2 \quad \dot{q}_3] \\ r^T &= [r_{d_1} \quad r_{d_2} \quad r_{d_3} \quad r_{d_4} \quad r_{d_5} \quad r_{d_6}] \\ &= [q_{d_1} \quad q_{d_2} \quad q_{d_3} \quad \dot{q}_{d_1} \quad \dot{q}_{d_2} \quad \dot{q}_{d_3}] \\ u^T &= [f_{hip} \quad \tau_{thigh} \quad \tau_{knee}] \end{aligned} \tag{38}$$

We define the normalized cost components as follows:

$$Cost_{Ei} = \frac{RMSE_i}{\max_{t\in[0,T]} |x_i - r_{d_i}|} \qquad Cost_{Uj} = \frac{RMSU_j}{\max_{t\in[0,T]} |u_j|} \tag{39}$$

The total tracking cost, total control cost, and total combined cost are finally defined as follows.

$$Cost_E = \sum_{i=1}^{6} Cost_{Ei} \quad , \quad Cost_U = \sum_{j=1}^{3} Cost_{Ui}$$
$$Cost = Cost_E + Cost_U \tag{40}$$

The *Cost* variable in the above equation is the objective function of the PSO algorithm.

SIMULATION RESULTS

The desired trajectory in this paper is walking data obtained by the Motion Studies Laboratory (MSL) of the Cleveland Department of Veterans Affairs Medical Center (VAMC) [11]. In this section we show the effectiveness of the proposed controller of Fig. 3 by performing simulation studies on the prosthesis robot model.

In the system model considered here, we have $q \in R^3$, so $M_r = \text{diag}(M_{11} \quad M_{22} \quad M_{33})$, $B_r = \text{diag}(B_{11} \quad B_{22} \quad B_{33})$, and $K_r = \text{diag}(K_{11} \quad K_{22} \quad K_{33})$. To obtain two equal real roots for each of joint displacements (critically damped responses for the hip vertical displacement q_1, and the thigh and knee angles q_2 and q_3) in the target impedance model of Eq. (8), B_{ii} must be equal to $2\sqrt{K_{ii}M_{ii}}$ and the two roots are both equal to $-\sqrt{K_{ii}/M_{ii}}$. To have two different real roots, B_{ii} must be greater than $2\sqrt{K_{ii}M_{ii}}$. We define the target impedance model with two real roots at −11 and −88 for the thigh, −5 and −94 for the knee, and −3 and −497 for the hip. We choose these values heuristically so that the target impedance model is stable, behaves similarly to an able-bodied leg, and results in good tracking. This approach results in the following impedance model matrices:

$$\begin{aligned} M_r &= \text{diag}\,(10 \quad 10 \quad 10) \\ K_r &= \text{diag}\,(15000 \quad 10000 \quad 5000) \\ B_r &= \text{diag}\,(5000 \quad 1000 \quad 1000) \end{aligned}$$

Particle Swarm Optimization

We use PSO to tune the controller and estimator parameters [38]. We use the following parameters for PSO: optimization problem dimension=14, number of iterations=20, population size=72, maximum rates for cognition and social learning=2.05, damping ratio for inertia rate=0.9, and scale factor=0.1.

We consider the following values for the minimum and maximum values of the search domain of μ, K_d, and λ:

$$\mu_i \in [0.001, \quad 0.01] \quad , \quad i = 1, \dots, 8$$
$$K_{d_i} \in [70, \quad 150] \quad , \quad i = 1, \dots, 3$$
$$\lambda_i \in [80, \quad 150] \quad , \quad i = 1, \dots, 3$$

where we use λ in Eqs. (9) and (10) to build the signal and error vectors, K_d in Eq. (21) to design the controller, and λ in Eq. (26) to design the update law. After some trial and error, we find good performance with boundary layer thicknesses for the trajectories s_Δ (shown in Fig. 2) for all joint displacements as $\varphi_1 = \varphi_2 = \varphi_3 = 0.5$. The initial state of the system is given as $\underline{x}_0{}^T = [0.019 \quad 1.13 \quad 0.09 \quad 0.09 \quad 0 \quad 1.6]$.

PSO decreases the $Cost$ of Eq. (40) from 3.44 at the initial generation to 3.16 at the 20th generation, which means that the total cost improves by 8%. Fig. 4 shows the best cost values over the 20 generations. The best solution found by PSO is given as follows:

- The robust term coefficients: $K_d = \text{diag}(89, \quad 117, \quad 103)$
- The adaptation rates:

$\mu = \text{diag}(0.003 \quad 0.01 \quad 0.009 \quad 0.005 \quad 0.005 \quad 0.01 \quad 0.007 \quad 0.01)$

- The sliding term coefficients: $\lambda = \text{diag}(105, \quad 121, \quad 98)$

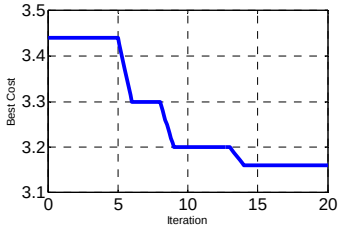

Fig. 4: PSO performance for finding optimal design parameters for the proposed controller

Robustness to System Model Parameter Variations

We assume that the treadmill parameters are constant so that $s_z = 0.905$ (meters), $k_b = 37000$ (N/m), and $\beta = 0.2$. However, we consider that the other system parameters are partially unknown to the controller and can vary ±30% from their nominal values. The ±30% parameter variation bounds are based on the authors' experience with the accuracy of motor parameter specifications. We list the nominal values of the system parameters in Table 1.

Fig. 5 compares the states of the closed-loop system with the desired trajectories (VAMC reference data) when values of the system parameters are varied ±30% relative to their nominal values. Fig. 5 shows that the controller tracks the desired trajectories not only with nominal parameter values, but also when the parameter values vary from their nominal values. This demonstrates good robustness for the control system.

Fig. 6 shows the control signals of the system (the active control force for the hip, and the active control torques for the thigh and knee) for the nominal parameter values, and also for the maximum and minimum deviations of the parameters. We see that the control magnitudes for the nominal case and the off-nominal cases are similar, which again demonstrates good robustness.

These results show that the controller structure is suitable for dealing with parameter variations without large changes in control effort. Note that high gain parameters in the target impedance model result in more accurate tracking but increases the magnitude of the control signals.

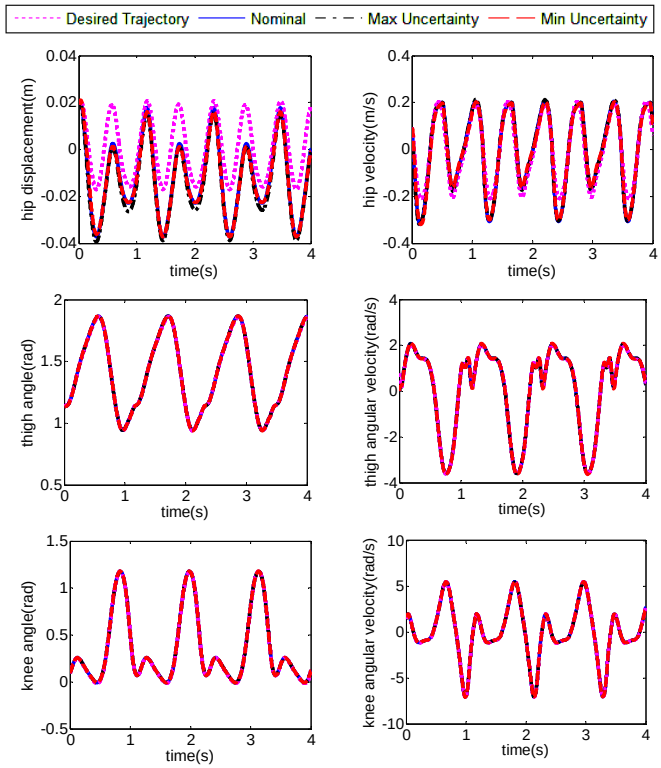

Fig. 5: Tracking performance: desired trajectory (magenta dotted line), response with nominal parameter values (blue solid line), response with +30% parameter deviations (black dash-dot line), and response with –30% parameter deviations (red dashed line)

Table 1: Nominal values of model parameters

Parameter	Description	Nominal Value	Units
m_1	Mass of link 1	40.5969	kg
m_2	Mass of link 2	8.5731	kg
m_3	Mass of link 3	2.29	kg
l_2	thigh length	0.425	m
l_3	Length from knee joint to bottom of shoe	0.527	m
c_2	Center of mass on thigh	0.09	m
c_3	Center of mass on shank	0.32	m
f	sliding friction in link 1	83.33	N
b	Rotary actuator damping	9.75	N-m-s
I_{2z}	Rotary inertia of link 2	0.138	kg-m^2
I_{3z}	Rotary inertia of link 3	0.0618	kg-m^2
g	acceleration of gravity	9.81	m/s^2

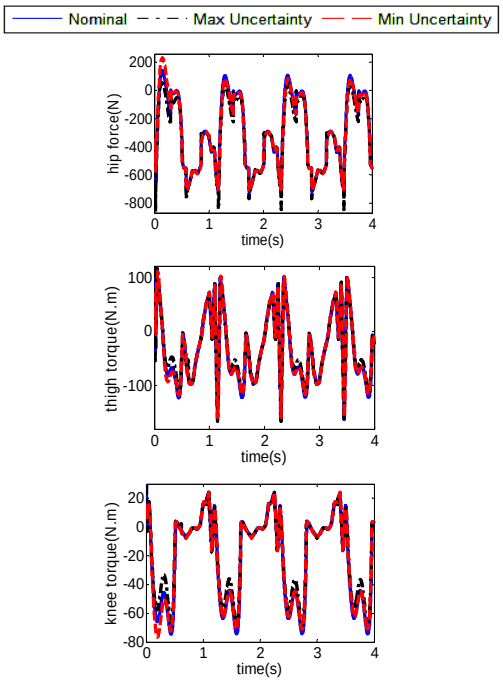

Fig. 6: Control signals: nominal system (blue solid line), +30% parameter deviations (black dash-dot line), and −30% parameter deviations (red dashed line)

Fig. 7 depicts the horizontal and vertical GRFs for different parameter values. We see that the generated forces appear similar to able-bodied GRFs. Fig. 7 shows that when the system parameters deviate from their nominal values by −30%, the mean of the squares of both F_X and F_z increase by 1%. When the system parameters deviate from their nominal values by +30%, the mean of the squares of F_X increase by 2% and F_z decreases by 12%.

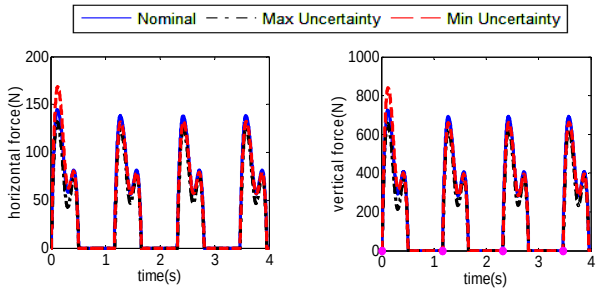

Fig. 7: The horizontal and vertical forces (GRFs) for nominal parameter values (blue solid line), +30% parameter deviations (black dash-dot line), and –30% parameter deviations (red dashed line). The heel strikes are shown in the right plot with circles on the x-axis

Table 2 summarizes the root mean square tracking error of each state, and the mean square value of each control signal ($RMSE_i$ and $RMSU_j$ respectively, as shown in Eqs. (36) and (37)), the normalized sum of each cost value ($Cost_E$ and $Cost_U$ from Eq. (39)), and the total cost ($Cost$ from Eq. (40)). Table 2 shows that there is not a large difference in $RMSE_i$ $(i = 1, \dots, 6)$ and $Cost_E$ whether the system parameters are at their nominal values, or at ±30% deviations, which again shows that the system demonstrates good robustness to parameter variations. Table 2 also shows that the total control cost and the total cost does not change by large amounts whether the system parameters are at their nominal values, or at ±30% deviations.

If the system parameters deviate by −30% from their nominal values, the total cost ($Cost$) increases by 1.6% and the tracking performance cost ($Cost_E$) increases by 2.5%. If the system parameters deviate by +30% from their nominal values, $Cost$ and $Cost_E$ increase by 2.6% and 6.5% respectively.

Table 2: The root mean squares of the tracking errors ($RMSE_i$) and control signals ($RMSU_i$), the total tracking error ($Cost_E$), the total control cost ($Cost_U$), and the total cost ($Cost$) for different values of the system parameters

	Nominal parameter values	Min parameter values (–30%)	Max parameter values (+30%)
$RMSE_1(m)$	0.0143	0.0146	0.0160
$RMSE_2(rad)$	0.0045	0.0048	0.0040
$RMSE_3(rad)$	0.0054	0.0055	0.0052
$RMSE_4(m/s)$	0.0460	0.0434	0.0449
$RMSE_5(rad/s)$	0.0448	0.0493	0.0482
$RMSE_6(rad/s)$	0.0248	0.0256	0.0364
$RMSU_1(N)$	388	389	396
$RMSU_2(N.m)$	68	69	63
$RMSU_3(N.m)$	36	36	32
$Cost_E$	2.02	2.07	2.15
$Cost_U$	1.14	1.14	1.08
$Cost$	3.16	3.21	3.24

Fig. 8 shows the trajectories of the estimated parameter vector p of Eq. (14) for the system for the nominal value of the system parameters, and also for the cases when the system parameters vary by ±30%. As anticipated, the parameter estimates do not perfectly match their true values, but exact parameter matching is not our goal; our goal is that the trajectories of s remain inside the boundary layer after the adaptation period, which is demonstrated in Fig. 9.

Fig. 9 also shows the trajectories of s_Δ as described in Eq. (24). Based on the values of φ_1, φ_2, φ_3, and s_Δ, it is seen that parameter adaptation is only active when the trajectories of s are outside the boundary layer; that is, when s_Δ is nonzero.

For instance, among the s trajectories for negative deviations of the system parameters in Fig. 9 (red dashed lines), the trajectory s for the hip is the only trajectory that exceeds the boundary layer (the region between $-\varphi_1 = -0.5$ and $+\varphi_1 = +0.5$), which occurs in $t \in [0.136, 0.326]$. The other trajectories s remain in the boundary layer. So the s_Δ trajectory for the hip is equal to $(s_{hip} - \varphi_1)$ as shown in Eq. (24), while the other s_Δ trajectories are zero. In this case the adaptation law of Eq. (26) is a function of only μ_i and the s_Δ trajectory for the hip.

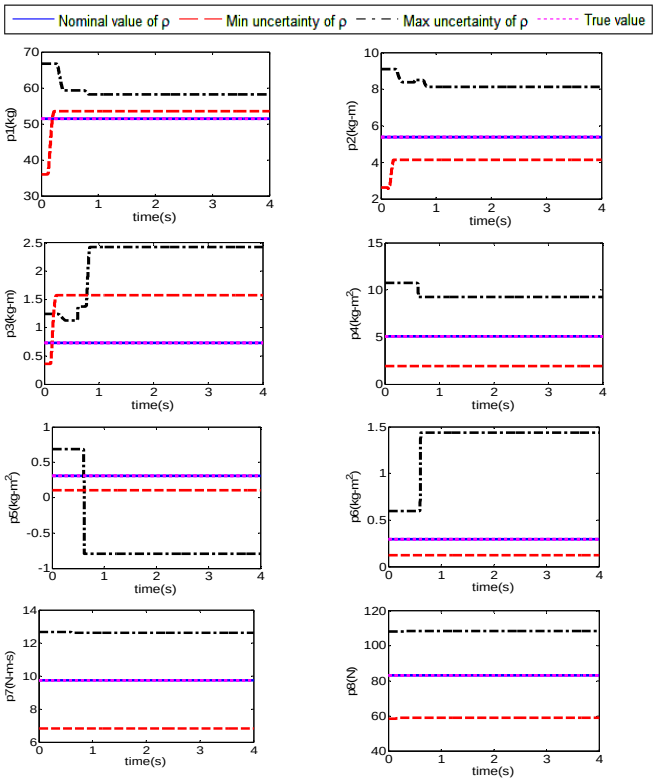

Fig. 8: Trajectories of the estimated parameter vector with nominal parameter values (blue solid line), +30% parameter deviations (black dash-dot line), and –30% parameter deviations (red dashed line). The true values are shown with magenta dotted lines

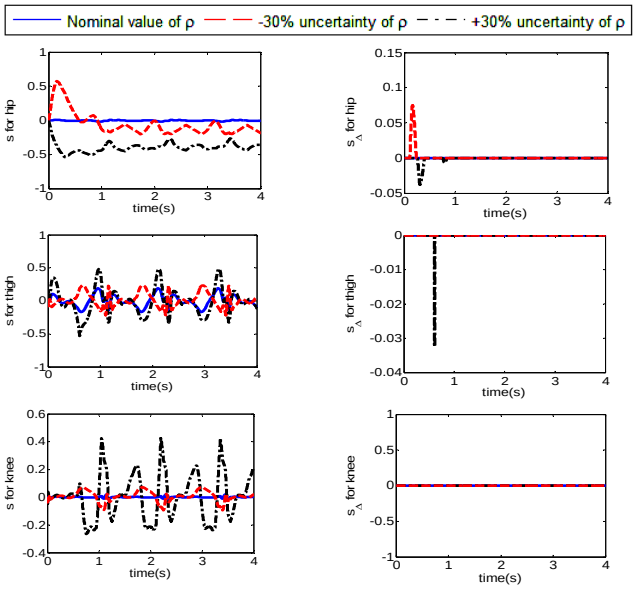

Fig. 9: Trajectories of s_Δ and s with nominal parameter values (blue solid line), +30% parameter deviations (black dash-dot line), and –30% parameter deviations (red dashed line)

CONCLUSIONS AND FUTURE WORK

We designed a regressor-based nonlinear robust model reference adaptive impedance controller for a prosthesis robot model. We first defined a target impedance model with two real poles for each degree of freedom. We then designed a robust model reference adaptive impedance controller, not only for estimating the uncertain parameters of the system, but also for driving the system trajectories to a boundary layer while compensating for the variations of GRF. We then proved the stability of the system for the non-scalar boundary layer trajectory case using Lyapunov theory and Barbalat's lemma. We used PSO to find the optimal control and estimator design parameters to minimize tracking error and control signal magnitude, which decreased the cost function by 8%.

We performed simulations with ±30% parameter deviations, and we saw that tracking performance remained accurate. Tracking errors for the nominal values of the parameter vector were 14 mm for the hip vertical displacement, 0.25 deg for the thigh angle, and 0.3 deg for the knee angle. We achieved fast transient responses with nominal parameter values and also with parameter deviations as large as ±30%.

With ±30 % parameter variations, the total cost increased by only 3%, which demonstrates good robustness. Although the parameter estimates did not converge to their true values, the trajectories of s remained inside their boundary layers after the adaptation period, which resulted in good robustness and tracking performance.

For future work, we will consider other important aspects of the proposed controller, including the following: the effect of the boundary layer thickness on system performance; and the robustness of the system to variations in the effect of GRFs. We will also pursue other designs of robust adaptive controllers to achive accurate parameter estimation and better tracking performance. We will also add the rotary and linear actuator models to the system to obtain the required voltages for driving DC motors. We will also implement the proposed method on a prosthetic leg prototype in the Control, Robotics and Mechatronics Lab at Cleveland State University. We will extend the controller to a 4-DOF model that includes an active ankle joint. Finally, we will use muli-objective optimization to achieve better tradeoffs of the tracking error costs and the control signal magnitudes. We will also design a continuous-time extended Kalman filter to estimate the states and GRFs of a 4-DOF prosthetic leg model and consider stability analisys of this filter.

Finally, we note that the results in this paper can be reproduced with Matlab code which is available at http://embeddedlab.csuohio.edu/Prosthetics/Adaptive.html.

ACKNOWLEDGMENTS

This research was supported by NSF Grant 1344954. The authors express their sincere gratitude to Jean-Jacques Slotine, Mojtaba Sharifi, Antonie van den Bogert, Elizabeth C. Hardin, and the anonymous reviewers for suggestions that improved the quality of this paper.

REFERENCES

[1] Ziegler-Graham, K., 2008, "Estimating the prevalence of limb loss in the United States: 2005 to 2050," Archives of Physical Medicine and Rehabilitation, vol. 89, no. 3, pp. 422‑429.

[2] Robbins, J.M. et al., 2008, "Mortality rates and diabetic foot ulcers," Journal of the American Podiatric Medical Association, vol. 98, no. 6, pp. 489-493.

[3] Sup,F., Varol, H.A., and Goldfarb, M., 2010, "Upslope walking with a powered knee and ankle prosthesis: initial results with an amputee subject," IEEE Transactions on Neural Systems and Rehabilitation Engineering, vol. 19, no. 1, pp. 71-78.

[4] Lawson, B. E., Varol, H.A., Goldfarb, M., 2011, "Standing stability enhancement with an intelligent powered transfemoral prosthesis," IEEE Transactions on Biomedical Engineering, vol. 58, no. 9, pp. 2617–2624.

[5] Hoover, C.D., Fulk, G.D., Fite, K.B., 2013, "Stair ascent with a powered transfemoral prosthesis under direct myoelectric control," IEEE/ASME Transactions on Mechatronics, vol. 18, no. 3, pp. 1191–1200.

[6] Sup, F., Varol H.A., Mitchell, J., Withrow, T.J., Goldfarb, M., 2009, "Preliminary evaluations of a self-contained anthropomorphic transfemoral prosthesis," IEEE ASME Trans Mechatron, vol. 14, no. 6, pp. 667–676.

[7] Fite, K., Mitchell, J., Sup, F., Goldfarb, M., 2007, "Design and control of an electrically powered knee prosthesis," IEEE 10th International Conference on Rehabilitation Robotics.

[8] Popovic, D., Oguztoreli, M.N., and Stein, R.B., 1991, "Optimal control for the active above-knee prosthesis," Annals of Biomedical Engineering, vol. 19, no. 2, pp. 131-150.

[9] Popovic, D., Tomovic, R., Tepavac, D., Schwirtlich, L., 1991, "Control aspects of active above-knee prosthesis", International Journal of Man-Machine Studies, vol. 35, no.6, pp. 751‑767.

[10] Sup, F., Bohara, A., and Goldfarb, M., 2008, "Design and control of a powered transfemoral prosthesis", International Journal of Robotics Research, vol. 27, no. 2, pp. 263-273.

[11] Khademi, G., Mohammadi, H., Hardin, E.C., Simon, D., 2015, "Evolutionary optimization of user intent recognition for transfemoral amputees," Submitted to: Biomedical Circuits and Systems Conference, Atlanta, Georgia, USA.

[12] Gregg, R.D., Sensinger, J.W., 2014, "Towards biomimetic virtual constraint control of a powered prosthetic leg," IEEE Transactions on Control Systems Technology, vol. 22, no. 1, pp. 246 – 254.

[13] Richter, H., Simon, D., and van den Bogert, A., 2014, "Semiactive virtual control method for robots with regenerative energy-storing joints,"19th , the International Federation of Automatic Control World Congress, Cape Town, South Africa.

[14] Richter, H. Simon, D., Smith, W, Samorezov, S., 2015, "Dynamic modeling, parameter estimation and control of a leg prosthesis test robot," Applied Mathematical Modelling, vol. 39, no. 12, pp. 559–573.

[15] Ott, C., Mukherjee, R., Nakamura, Y., 2010 "Unified impedance and admittance control," IEEE International Conference on Robotics and Automation, 554–561.

[16] Abdossalami, A., Sirouspour, S., 2009, "Adaptive control for improved transparency in haptic simulations," IEEE Transactions on Haptics, vol. 2, no. 1, pp. 2–14.

[17] Hogan, N., 1985, "Impedance control: An approach to manipulation: Part I, Part II and Part III,"ASME J. Dynamic Syst. Measurement, Contr., vol. 107, no.1, pp. 1-24.

[18] Chan, S.P., Yao, B., Gao, W.B., Cheng, M., 1991, "Robust impedance control of robot manipulators," International J. of Robotics and Automation, vol. 6, no. 4, pp. 220-227.

[19] Mohammadi, H., Richter, H., 2015, "Robust Tracking/Impedance Control: Application to Prosthetics," American Control Conference, Chicago, Illinois.

[20] Hussain, S., Xie, S.Q., and Jamwal, P.K., 2013, "Adaptive impedance control of a robotic orthosis for gait rehabilitation," IEEE Transactions on Cybernetics, vol. 43 , no. 3, pp. 1025-1034.

[21] Sharifi, M., Behzadipour, S., Vossoughi, G., 2014, "Nonlinear model reference adaptive impedance control for human–robot interactions," Control Engineering Practice, vol. 32, no. 8, pp. 9-27.

[22] Park, H., Lee, J., 2004, "Adaptive impedance control of a haptic interface," Mechatronics, vol. 14, no. 3, pp. 237‑253.

[23] Zhijun, L., Ge, S.S., 2013, "Adaptive robust controls of biped robots," Control Theory & Applications, IET, vol. 7, no. 2, pp. 161-175.

[24] Tomei, P., 2000, "Robust adaptive friction compensation for tracking control of robot manipulators," IEEE Transactions on Automatic Control, vol. 45, no. 11, pp. 2164-2169.

[25] Huh, S.-H., Bien, Z., 2007, "Robust sliding mode control of a robot manipulator based on variable structure-model reference adaptive control approach," IET Control Theory & Applications, vol. 1 ,no. 5, pp. 1355-1363.

[26] Moosavi, M., Eram, M., Khajeh, A., Mahmoudi, O., Piltan, F., 2013, "Design new artificial intelligence base modified PID hybrid controller for highly nonlinear system," International Journal of Advanced Science and Technology, vol. 57, no. 5, pp. 45-62.

[27] Salehi, A., Piltan, F., Mousavi, M., Khajeh, A., Rashidian, M., 2013, "Intelligent robust feed-forward fuzzy feedback linearization estimation of PID control with application to continuum robot," International Journal of Information Engineering and Electronic Business, vol. 5, no. 1, pp. 1-16.

[28] Azimi, V., Menhaj, M. B., Fakharian, A., 2015, "Tool position tracking control of a nonlinear uncertain flexible robot manipulator by using robust H2 /H∞ controller via T–S fuzzy model," Sadhana, vol. 40, no. 2, pp. 307-333.

[29] Azimi, V., Fakharian, A., Menhaj M. B., 2013, "Position and current control of an permanent-magnet synchronous motor by using loop-shaping methodology: blending of H∞ mixed-sensitivity problem and T-S fuzzy model scheme," Journal of Dynamic Systems Measurement and Control-Transactions of the ASME, vol.135, no. 5, pp. 051006-1–051006-11.

[30] Azimi, V., Nekoui, M. A., Fakharian, A., 2012, "Robust multi-objective H2/ H∞ tracking control based on T-S fuzzy model for a class of nonlinear uncertain drive systems," Proceeding of the Institution of Mech. Eng. Part I-Journal of Systems and Control Engineering, vol. 226, no. 8, pp. 1107–1118.

[31] Slotine, J.-J. E., Coetsee, J. A., 1986, "Adaptive sliding controller synthesis for non-linear systems," International Journal of Control, vol. 43, no. 6, pp. 1631-1651.

[32] Sanner, R.M., Slotine, J.-J. E., 1992, "Gaussian networks for direct adaptive control," IEEE Transactions on Neural Networks, vol.3 , no. 6 , pp. 837-863.

[33] Slotine, J.-J. E., Li, W., 1987, "Adaptive strategy in constrained manipulators," IEEE International Conference on Robotics and Automation.

[34] Slotine, J.-J. E., Li, W., 1988, "Adaptive manipulator control: a study case," IEEE Transactions on Automatic Control, vol. 33, no. 11, pp. 995-1003.

[35] Richter, H., Simon, D., 2014, "Robust tracking control of a prosthesis test robot," J. Dyn. Sys., Meas., Control , vol. 136, no. 3, doi: 10.1115/1.4026342.

[36] Slotine, J.-J. E., Li, W., 1991, Applied nonlinear control, NJ: Prentice-Hall.

[37] Huang, A.-C., Chien, M.-C., 2010, "Adaptive control of robot manipulators," World Scientific Publishing Co.

[38] Simon, D., 2013, Evolutionary optimization algorithms, John Wiley & Sons.